COMPUTATIONAL ASPECTS OF DUAL-POROSITY MODELS

Todd Arbogast*

January 11, 1996

Introduction

Macroscopic microstructure models of dual-porosity type model, among other things, the flow of fluids in highly fractured porous media; that is, media comprised of porous matrix rock divided into relatively small blocks by thin fractures [7], [11], [1], [6], [9], [5], [3]. Mathematically, a dual-porosity model is derived by homogenization of the mesoscopic equations (i.e., the Darcy-scale description that explicitly models flow within the fractures and matrix). This results in a relatively complex system of partial differential equations in seven variables, (t, x, y). At first glance, it may not be apparent that there is any advantage to the macroscopic description versus the mesoscopic. However, the dual-porosity model explicitly captures the length scales of the physical problem, and is thus much easier to approximate computationally.

For example, single-phase flow is governed on the mesoscopic scale by a parabolic equation that is relatively easy to approximate; however, the grid must be extremely fine to resolve the fractures. Fractures are on the order of 100 micrometers wide, and matrix blocks are on the order of a meter wide. In three space dimensions, a uniform grid would require about a trillion grid elements to resolve the flow in a *single* matrix block. A graded grid would be more efficient, but would still require over a thousand elements per matrix block. There may be many millions of matrix blocks in an entire reservoir or aquifer, so many billions of grid elements are required to resolve the length scales of the mesoscopic system. The enormous amount of computational resources required to solve this time dependent problem render it intractable.

On the other hand, as we discuss in this paper, the homogenized, dual-porosity model requires far less computational effort to solve numerically, and it approximates well the mesoscopic model.

1 Single-phase flow

In this section we consider the problem of approximating a linear dual-porosity model of the flow of a single, compressible fluid phase in a naturally fractured reservoir or aquifer. Further details can be found in the papers [1], [9], [6], and [5]. The numerical technique described here can be extended to nonlinear problems, as we describe in the next section on two-phase flow.

*Department of Mathematics, Texas Institute for Computational and Applied Mathematics, The University of Texas at Austin, Austin, Texas 78712.

1.1 The mesoscopic and dual-porosity models

The single-phase model we consider is relatively simple so that we can illustrate our numerical techniques. We restrict to a linear set of equations and ignore gravity. In practice, gravitational effects are quite important, so we must include them [4]; this has been done in the computational examples to follow.

As is usual in homogenization, Ω is the reservoir or aquifer domain, assumed to be periodic with period ε. To simplify the description of the physical scaling, we assume that ε is the dimensionless fracture spacing, $\varepsilon = 1$ in Ω, and, as usual, homogenization takes $\varepsilon \to 0$. The unit cell is $Y = (0,1)^3$ containing a single porous solid matrix block M and the surrounding fracture set F ($\bar{M} \cup F = Y$, $F \cap M = \emptyset$, and $\partial M \subset Y$). The matrix and fracture parts of Ω are M^ε and F^ε, respectively, defined by

$$M^\varepsilon = \Omega \cap \bigcup_{i=1}^{N(\varepsilon)} M_i^\varepsilon, \quad F^\varepsilon = \Omega \cap \bigcup_{i=1}^{N(\varepsilon)} F_i^\varepsilon, \tag{1.1}$$

where M_i^ε and F_i^ε are the ε-size copies of M and F covering Ω.

The reservoir Ω is periodic since its porosity ϕ_ε and permeability k_ε are periodically discontinuous over Ω as we go from matrix to fracture:

$$\begin{cases} k_\varepsilon(x) = \varepsilon^2 k_M, \quad \phi_\varepsilon(x) = \phi_M & \text{in } M^\varepsilon, \\ k_\varepsilon(x) = k_F, \quad \phi_\varepsilon(x) = \phi_F & \text{in } F^\varepsilon, \end{cases} \tag{1.2}$$

where ϕ_M, ϕ_F are positive constants, and k_M, k_F are positive definite tensors (they could also depend on x and y). To simplify the discussion, we restrict the model to be linear in the density ρ by assuming the equation of state

$$\rho(p) = \rho_0 \, e^{c(p-p_0)}, \tag{1.3}$$

where p is the pressure, c is the fluid (i.e., liquid) compressibility, and subscript 0 denotes a reference quantity. The mesoscopic equation is then simply

$$\phi_\varepsilon \frac{\partial \rho^\varepsilon}{\partial t} - \nabla \cdot \left(\frac{k_\varepsilon}{\mu c} \nabla \rho^\varepsilon \right) = f \quad \text{in } (0,T) \times \Omega, \tag{1.4}$$

plus appropriate initial and boundary conditions, where μ is the fluid viscosity and f represents the injection and extraction wells.

Homogenization yields the dual-porosity model for the fracture density $\rho_F(t,x)$ and the matrix density $\rho_M(t,x,y)$ [6], [5]. Fractures flow is described by

$$\phi^* \frac{\partial \rho_F}{\partial t} + \frac{\phi_M}{|Y|} \int_M \frac{\partial \rho_M}{\partial t}(t,x,y)\, dy - \nabla_x \cdot \left(\frac{k^*}{\mu c} \nabla_x \rho_F \right) = f \quad \text{in } (0,T) \times \Omega, \tag{1.5}$$

where $\phi^* = (|F|/|Y|)\phi_F$ and k^* is the homogenized permeability tensor defined by its entries

$$k_{ij}^* = \frac{1}{|Y|} \int_F k_F \, (\vec{e}_i + \nabla_y \lambda_i) \cdot (\vec{e}_j + \nabla_y \lambda_j)\, dy, \tag{1.6}$$

where $\lambda_i(y)$ are the unique periodic solutions in $H^1(F)$ (modulo constants) of the cell problems

$$\begin{cases} -\nabla_y \cdot k_F \, (\vec{e}_i + \nabla_y \lambda_i(y)) = 0 & \text{in } F, \\ k_F \, (\vec{e}_i + \nabla_y \lambda_i(y)) \cdot \vec{\nu} = 0 & \text{on } \partial M, \end{cases} \tag{1.7}$$

with $\{\vec{e}_i\}_{1\le i\le N}$ the canonical basis of $\mathbb{R}^N$. Matrix flow is described by

$$\begin{cases} \phi_M \dfrac{\partial \rho_M}{\partial t} - \nabla_y \cdot \left(\dfrac{k_M}{\mu c} \nabla_y \rho_M \right) = f(t,x) & \text{in } (0,T)\times\Omega\times M, \\ \rho_M(t,x,y) = \rho_F(t,x) & \text{on } (0,T)\times\Omega\times\partial M. \end{cases} \tag{1.8}$$

1.2 Numerical solution

To discretize time, we select a series of time levels

$$0 = t^0 < t^1 < t^2 < \ldots < t^N.$$

A backward Euler time approximation of (1.8) results in the semi-discrete equations

$$\begin{cases} \phi_M \dfrac{\rho_M^n - \rho_M^{n-1}}{t^n - t^{n-1}} - \nabla_y \cdot \left(\dfrac{k_M}{\mu c} \nabla_y \rho_M^n \right) = f(t^n,x) & \text{in } \Omega\times M, \\ \rho_M^n(x,y) = \rho_F^n(x) & \text{on } \Omega\times\partial M. \end{cases} \tag{1.9}$$

This is a linear partial differential equation in y for each fixed x, and $\rho_F^n(x)$ is a single parameter to the system. Therefore, we can express the solution as an affine operator of ρ_F^n by computing the derivative of the system with respect to ρ_F^n and finding the solution for any particular choice of ρ_F^n (such as 0) [1], [9]. That is, for fixed x, we find the solution $\tilde{\rho}_M^n(x,y)$ to

$$\begin{cases} \phi_M \dfrac{\tilde{\rho}_M^n}{t^n - t^{n-1}} - \nabla_y \cdot \left(\dfrac{k_M}{\mu c} \nabla_y \tilde{\rho}_M^n \right) = 0 & \text{in } \Omega\times M, \\ \tilde{\rho}_M^n(x,y) = 1 & \text{on } \Omega\times\partial M, \end{cases} \tag{1.10}$$

and the solution $\bar{\rho}_M^n(x,y)$ to

$$\begin{cases} \phi_M \dfrac{\bar{\rho}_M^n - \rho_M^{n-1}}{t^n - t^{n-1}} - \nabla_y \cdot \left(\dfrac{k_M}{\mu c} \nabla_y \bar{\rho}_M^n \right) = f(t^n,x) & \text{in } \Omega\times M, \\ \bar{\rho}_M^n(x,y) = 0 & \text{on } \Omega\times\partial M. \end{cases} \tag{1.11}$$

Then we have

$$\rho_M^n(x,y) = \rho_F^n(x)\,\tilde{\rho}_M^n(x,y) + \bar{\rho}_M^n(x,y), \tag{1.12}$$

and the matrix equations have been decoupled from the fracture equations. Now (1.5) is approximated semi-discretely as

$$\begin{aligned} \phi^* \frac{\rho_F^n - \rho_F^{n-1}}{t^n - t^{n-1}} + \left(\frac{\phi_M}{|Y|} \int_M \frac{\tilde{\rho}_M^n(x,y)}{t^n - t^{n-1}}\, dy \right) \rho_F^n + \frac{\phi_M}{|Y|} \int_M \frac{\bar{\rho}_M^n(x,y) - \rho_M^{n-1}(x,y)}{t^n - t^{n-1}}\, dy \\ -\nabla_x \cdot \left(\frac{k^*}{\mu c} \nabla_x \rho_F^n \right) = f(t^n,x) \quad \text{in } \Omega. \end{aligned} \tag{1.13}$$

Altogether, (1.10)–(1.13) is simply a backward Euler, semi-discrete approximation of (1.5), (1.8) written in a decoupled form.

To (1.10)–(1.13), we apply any appropriate spatial discretization (Galerkin finite elements, finite differences, mixed finite element methods, collocation, finite volume methods, etc.). The solution algorithm is then as follows.

1. Find ρ_F^0 and ρ_M^0 from the initial conditions.
2. For each $n = 1, 2, ..., N$:
   (a) Solve for $\tilde{\rho}_M^n$ and $\bar{\rho}_M^n$ from ρ_M^{n-1} and (1.10)–(1.11) *only* at the x-points where the discrete scheme requires a value;
   (b) Solve for ρ_F^n from ρ_F^{n-1}, $\tilde{\rho}_M^n$, $\bar{\rho}_M^n$, ρ_M^{n-1}, and (1.13);
   (c) Define ρ_M^n from ρ_F^n, $\tilde{\rho}_M^n$, $\bar{\rho}_M^n$, and (1.12).

We note that the matrix equations can be solved in parallel quite naturally. Also, if we consider the discretization of the original equations (1.5), (1.8), then our decomposition is a simple and parallel way to form the Shur complement system that arises when the matrix unknowns are eliminated.

Recall that the mesoscopic equations would require the solution of a single coupled system on a grid with perhaps billions of grid elements. In contrast, the dual-porosity system requires the solution of a single large fracture system and many small, decoupled matrix problems. The fracture equations can be solved on a grid with spacing much larger than the fracture spacing, say on the order of 1 to 100 meters, so that perhaps 100,000 grid elements are needed. Depending on the spatial discretization, we need to approximate matrix flow in roughly one matrix block per grid element (*not* in every matrix block!). The two sub-problems on each matrix block are small, physically symmetric, and uniformly parabolic; thus, a relatively coarse grid can be used of perhaps less than 100 grid elements (in fact, good results are sometimes reported using as few as one grid element per matrix block). The total number of grid points involved in the system is on the order of 20 million, a considerable savings over the mesoscopic system. The real advantage of the dual-porosity approach, however, is that the length scales have been explicitly modeled. We have a relatively easy time solving the matrix flow (possibly even in parallel) and only need to invest substantial computational resources in the coupled fracture calculation, which is thousands of times smaller than the coupled mesoscopic problem.

2 Two-phase flow

We now consider the problem of approximating a highly nonlinear, dual-porosity model of the flow of two completely immiscible, incompressible fluid phases in a naturally fractured reservoir or aquifer. Further details can be found in the papers [3], [9], and [5].

2.1 The mesoscopic and dual-porosity models

Although the effects of compressibility can be taken into account [3], we will assume incompressible media and fluids. In that case, the equations for the wetting fluid phase α and the non-wetting fluid phase β can be easily described when gravitational effects are taken into account.

Each fluid phase $\xi = \alpha$ or β has its own pressure p_ξ, (constant) density ρ_ξ, viscosity μ_ξ, and saturation S_ξ. We also define the phase *potentials* Φ_ξ as

$$\Phi_\xi = p_\xi - \rho_\xi \, g \, z(x),$$

where g is the gravitational constant and $z(x)$ is the depth of point x.

The material properties are again discontinuous over the domain Ω as we go from matrix to fracture. This includes the porosity ϕ_ε and permeability k_ε, but also now the functions giving the relative permeability $k_{r\xi,\varepsilon}(S_\alpha)$, $\xi = \alpha, \beta$, and the capillary pressure $p_{c,\varepsilon}(S_\alpha)$. We must also scale the absolute permeability by ε^2 as in Equation (1.2) and the gravitational terms by ε^{-1} in the matrix as we describe below.

The mesoscopic equations consist of two phase conservation equations, the definitions of the two phase potentials, a capillary pressure relation, and a volume balance equation. The two phase equations are a combination of the two-phase generalization of the Darcy law and conservation of mass (or volume). Since Darcy's law gives the phase velocities as

$$-\frac{k_\varepsilon k_{r\xi,\varepsilon}(S^\varepsilon_\alpha)}{\mu_\xi}\nabla\Phi^\varepsilon_\xi = -\frac{k_\varepsilon k_{r\xi,\varepsilon}(S^\varepsilon_\alpha)}{\mu_\xi}(\nabla p^\varepsilon_\xi - \rho_\xi g \nabla z_\varepsilon),$$

the full set of equations is

$$\begin{cases} \phi_\varepsilon \dfrac{\partial S^\varepsilon_\xi}{\partial t} - \nabla\cdot\left(\dfrac{k_\varepsilon k_{r\xi,\varepsilon}(S^\varepsilon_\alpha)}{\mu_\xi}\nabla\Phi^\varepsilon_\xi\right) = f_\xi, & \text{in } (0,T)\times\Omega,\ \xi=\alpha,\beta,\\ \Phi^\varepsilon_\xi = p^\varepsilon_\xi - \rho_\xi\, g\, z(x), & \text{in } (0,T)\times F^\varepsilon,\ \xi=\alpha,\beta,\\ \Phi^\varepsilon_\xi = p^\varepsilon_\xi - \rho_\xi\, g\, z(x^\varepsilon_c + \varepsilon^{-1}(x-x^\varepsilon_c)) + \Phi^\varepsilon_{\xi,0}, & \text{in } (0,T)\times M^\varepsilon,\ \xi=\alpha,\beta,\\ p_{c,\varepsilon}(S^\varepsilon_\alpha) = p^\varepsilon_\beta - p^\varepsilon_\alpha, & \text{in } (0,T)\times\Omega,\\ S^\varepsilon_\alpha + S^\varepsilon_\beta = 1, & \text{in } (0,T)\times\Omega, \end{cases} \tag{2.14}$$

plus appropriate initial and boundary conditions, where $x^\varepsilon_c(x)$ is the centroid of the block containing x and $\Phi^\varepsilon_{\xi,0}$ is a reference potential. We have scaled the depth in the definition of the potentials in the matrix so that gravitational effects do not lose strength as we homogenize [3]. We must also account for the fact that a potential has no absolute scale by explicitly defining the reference potentials as follows. Set $\Phi^\varepsilon_{\beta,0} = 0$ and define $\Phi^\varepsilon_{\alpha,0}(t,x)$ by requiring

$$\begin{cases} \displaystyle\int_{M^\varepsilon(x)} p^{-1}_{c,M}(\bar\Phi^\varepsilon_\beta - \bar\Phi^\varepsilon_\alpha + \Phi^\varepsilon_{\alpha,0}(t,x) + (\rho_\beta-\rho_\alpha)\, g\, z(x^\varepsilon_c + \varepsilon^{-1}(X - x^\varepsilon_c)))\, dX\\ \quad = \displaystyle\int_{M^\varepsilon(x)} p^{-1}_{c,M}(\bar\Phi^\varepsilon_\beta - \bar\Phi^\varepsilon_\alpha + (\rho_\beta-\rho_\alpha)\, g\, z(X))\, dX,\\ \bar\Phi^\varepsilon_\xi = \dfrac{1}{|\partial M^\varepsilon(x)|}\displaystyle\int_{\partial M^\varepsilon(x)} \Phi^\varepsilon_\xi\, da(X), \end{cases} \tag{2.15}$$

where $S^\varepsilon(x)$ is the matrix block containing x. This procedure maintains a proper relationship between the matrix and fracture potentials as we homogenize, by balancing mass through the capillary pressure relation. Note that when $\varepsilon = 1$, we have the expected mesoscopic equations.

Formal homogenization [3] leads to a set of dual-porosity equations that govern the fracture $p_{\xi F}(t,x)$, $\Phi_{\xi F}(t,x)$, and $S_{\xi F}(t,x)$ and the matrix $p_{\xi M}(t,x,y)$, $\Phi_{\xi M}(t,x,y)$, and $S_{\xi M}(t,x,y)$. The fracture equations in $(0,T)\times\Omega$ are

$$\begin{cases} \phi^* \dfrac{\partial S_{\xi F}}{\partial t} + \dfrac{\phi_M}{|Y|}\displaystyle\int_M \frac{\partial S_{\xi M}}{\partial t}(t,x,y)\, dy - \nabla\cdot\left(\dfrac{k^* k_{r\xi F}(S_{\alpha F})}{\mu_\xi}\nabla\Phi_{\xi F}\right) = f_\xi, & \xi=\alpha,\beta,\\ \Phi^\varepsilon_{\xi F} = p_{\xi F} - \rho_\xi\, g\, z(x), & \xi=\alpha,\beta,\\ p_{cF}(S_{\alpha F}) = p_{\beta F} - p_{\alpha F},\\ S_{\alpha F} + S_{\beta F} = 1, \end{cases} \tag{2.16}$$

where ϕ^* and k^* are as in the single-phase case. The matrix equations are

$$\begin{cases} \phi_M \dfrac{\partial S_{\xi M}}{\partial t} - \nabla \cdot \left(\dfrac{k_M k_{r\xi M}(S_{\alpha M})}{\mu_\xi} \nabla \Phi_{\xi M} \right) = f_\xi(t,x) & \text{in } (0,T)\times\Omega\times M,\ \xi=\alpha,\beta, \\ \Phi^\varepsilon_{\xi M} = p_{\xi M} - \rho_\xi\, g\, z(x+y-y_c) + \Phi_{\xi,0}, & \text{in } (0,T)\times F^\varepsilon,\ \xi=\alpha,\beta, \\ p_{cM}(S_{\alpha M}) = p_{\beta M} - p_{\alpha M} & \text{in } (0,T)\times\Omega\times M, \\ S_{\alpha M} + S_{\beta M} = 1 & \text{in } (0,T)\times\Omega\times M, \\ \Phi_{\xi M}(t,x,y) = \Phi_{\xi F}(t,x) & \text{on } (0,T)\times\Omega\times\partial M, \end{cases} \tag{2.17}$$

where y_c is the centroid of Y. Note that the boundary condition on ∂M requires continuity of potential, not pressure as might be expected. The reference potential is defined by setting $\Phi_{\beta,0} = 0$ and requiring $\Phi_{\alpha,0}(t,x)$ to satisfy

$$\int_M p_{c,M}^{-1}(\Phi_{\beta F} - \Phi_{\alpha F} + \Phi_{\alpha,0} + (\rho_\beta - \rho_\alpha)\, g\, z(x+y-y_c))\, dy = |M| S_{\alpha F}. \tag{2.18}$$

2.2 Numerical solution

Although each of the systems (2.14)–(2.18) is posed with 7 independent variables, two phase pressures, potentials, and saturations, and $\Phi_{\alpha,0}$, we can reduce this number to two. The reference potential is zero in the mesoscopic equations (with $\varepsilon = 1$, and it changes very slowly in the dual-porosity case; thus we can use its old value when solving for the other variables, and then update it at the end of the time step using (2.18). Using the volume balance relation, we can eliminate one of the saturations; moreover, the capillary pressure relation allows us to eliminate the other saturation (or either of the two pressures, but for simplicity, let us assume that we eliminate both saturations). That is, the saturations are functions of the appropriate pressures:

$$S_\alpha = p_c^{-1}(p_\beta - p_\alpha) \quad \text{and} \quad S_\beta = 1 - S_\alpha.$$

Finally, the potentials are also functions of the pressures and can be eliminated. We are thus left only to discretize the nonlinear partial differential equations.

Again we use a backward Euler time discretization on the complete system (2.16)–(2.17). For the matrix, we obtain equations similar to (1.9). For time level t^n, we have partial differential equations in y for each fixed x for the matrix pressures $p^n_{\alpha M}(x,y)$ and $p^n_{\beta M}(x,y)$ with $p^n_{\alpha F}(x)$ and $p^n_{\beta F}(x)$ as two parameters to the system. Our decoupling strategy cannot be applied directly to these equations, however, since they are nonlinear.

We further discretize (2.16)–(2.17) in space by applying Galerkin finite elements, finite differences, or some other appropriate method. This reduces the system to a fully discrete, finite dimensional problem. Let the number of fracture unknowns be I, and denote them at time level t^n by

$$\vec{p}^{\,n}_{\xi F} = \{p^n_{\xi F,i},\ i = 1,2,...,I\}, \quad \xi = \alpha,\beta.$$

Usually, $p^n_{\xi F,i}$ will be an approximation to $p^n_{\xi F}$ at grid point i. For the purposes of exposition, assume this to be the case, and also that the numerical method only requires a matrix block at each grid point, as in Figure 1. Then associated to each grid point $i = 1,2,...,I$, we have a series of matrix unknowns

$$\vec{p}_{\xi M,i} = \{p_{\xi M,ij},\ j = 1,2,...,J_i\}, \quad \xi = \alpha,\beta,$$

in the ith matrix block. Let

$$\vec{p}_{\xi M} = \{p_{\xi M,ij},\ i = 1,2,...,I,\ j = 1,2,...,J_i\}, \quad \xi = \alpha, \beta.$$

The fully discrete nonlinear equations then take the form

$$\begin{cases} \mathcal{F}_i(\vec{p}^{\,n}_{\alpha F}, \vec{p}^{\,n}_{\beta F}, \vec{p}^{\,n}_{\alpha M}, \vec{p}^{\,n}_{\beta M}) = 0, & i = 1,2,...,I, \\ \mathcal{M}_{ij}(p^n_{\alpha F,i}, p^n_{\beta F,i}, \vec{p}^{\,n}_{\alpha M,i}, \vec{p}^{\,n}_{\beta M,i}) = 0, & i = 1,2,...,I,\ j = 1,2,...,J_i, \end{cases} \tag{2.19}$$

for some nonlinear functions $\mathcal{F}_i$ and $\mathcal{M}_{ij}$.

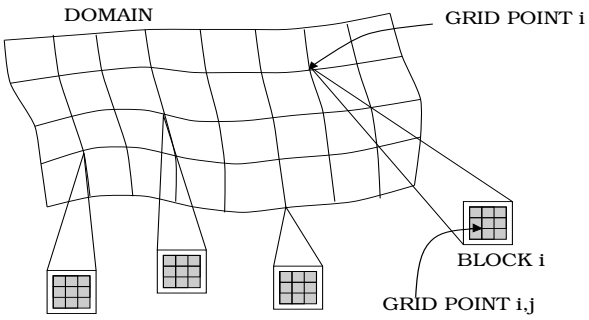

Figure 1: The discrete grid.

One way to solve nonlinear equations of this form is to use Newton's method to linearize it. Let

$$\vec{p}^{\,n,m}_{\xi F} \quad \text{and} \quad \vec{p}^{\,n,m}_{\xi M}, \quad \xi = \alpha, \beta,$$

denote the mth Newton iterate for the nth time level's solution, let D_π denote partial differentiation with respect to π, and let

$$\mathcal{F}^{n,m-1}_i = \mathcal{F}_i(\vec{p}^{\,n,m-1}_{\alpha F}, \vec{p}^{\,n,m-1}_{\beta F}, \vec{p}^{\,n,m-1}_{\alpha M}, \vec{p}^{\,n,m-1}_{\beta M}),$$
$$\mathcal{M}^{n,m-1}_{ij} = \mathcal{M}_{ij}(p^{n,m-1}_{\alpha F,i}, p^{n,m-1}_{\beta F,i}, \vec{p}^{\,n,m-1}_{\alpha M,i}, \vec{p}^{\,n,m-1}_{\beta M,i}),$$

and similarly for the derivatives. Then we can describe the Newton procedure as the following iterative process.

1. Start with an initial guess for the solution

$$\vec{p}^{\,n,0}_{\xi F}, \quad \vec{p}^{\,n,0}_{\xi M}, \quad \xi = \alpha, \beta.$$

2. For each $m = 1,2,...$ until convergence is reached:

   (a) Solve for

$$\delta\vec{p}^{\,n,m}_{\xi F}, \quad \delta\vec{p}^{\,n,m}_{\xi M}, \quad \xi = \alpha, \beta,$$

satisfying

$$\begin{cases} \mathcal{F}_i^{n,m-1} + \sum_{i'} \Big\{ D_{p_{\alpha F,i'}} \mathcal{F}_i^{n,m-1} \delta p_{\alpha F,i'}^{n,m} + D_{p_{\beta F,i'}} \mathcal{F}_i^{n,m-1} \delta p_{\beta F,i'}^{n,m} \\ \qquad + \sum_{j'} \Big[D_{p_{\alpha M,i'j'}} \mathcal{F}_i^{n,m-1} \delta p_{\alpha M,i'j'}^{n,m} + D_{p_{\beta M,i'j'}} \mathcal{F}_i^{n,m-1} \delta p_{\beta M,i'j'}^{n,m} \Big] \Big\} \\ \quad = 0, \quad i = 1,2,...,I, \\ \mathcal{M}_{ij}^{n,m-1} + D_{p_{\alpha F,i}} \mathcal{M}_{ij}^{n,m-1} \delta p_{\alpha F,i}^{n,m} + D_{p_{\beta F,i}} \mathcal{M}_{ij}^{n,m-1} \delta p_{\beta F,i}^{n,m} \\ \qquad + \sum_{j'} \Big[D_{p_{\alpha M,ij'}} \mathcal{M}_{ij}^{n,m-1} \delta p_{\alpha M,ij'}^{n,m} + D_{p_{\beta M,ij'}} \mathcal{M}_{ij}^{n,m-1} \delta p_{\beta M,ij'}^{n,m} \Big] \\ \quad = 0, \quad i = 1,2,...,I, \ j = 1,2,...,J_i; \end{cases} \tag{2.20}$$

(b) Define

$$\vec{p}_{\xi F}^{\,n,m} = \vec{p}_{\xi F}^{\,n,m-1} + \delta \vec{p}_{\xi F}^{\,n,m}, \quad \vec{p}_{\xi M}^{\,n,m} = \vec{p}_{\xi M}^{\,n,m-1} + \delta \vec{p}_{\xi M}^{\,n,m}, \quad \xi = \alpha, \beta.$$

Within the linearized Newton problem, the matrix solution in the ith block is an affine operator of $p_{\alpha F,i}^{n,m}$ and $p_{\beta F,i}^{n,m}$. Therefore, we can again decouple the matrix and fracture problems as in the last section [10]. We replace the matrix problem in (2.20) above by the following three problems for

$$(\tilde{\delta}\vec{p}_{\alpha M,i}^{\,n,m}, \tilde{\delta}\vec{p}_{\beta M,i}^{\,n,m}), \quad (\hat{\delta}\vec{p}_{\alpha M,i}^{\,n,m}, \hat{\delta}\vec{p}_{\beta M,i}^{\,n,m}), \quad \text{and} \quad (\bar{\delta}\vec{p}_{\alpha M,i}^{\,n,m}, \bar{\delta}\vec{p}_{\beta M,i}^{\,n,m}).$$

For each $i = 1,2,...,I$ and $j = 1,2,...,J_i$,

$$\begin{cases} D_{p_{\alpha F,i}} \mathcal{M}_{ij}^{n,m-1} + \sum_{j'} \Big[D_{p_{\alpha M,ij'}} \mathcal{M}_{ij}^{n,m-1} \tilde{\delta} p_{\alpha M,ij'}^{n,m} + D_{p_{\beta M,ij'}} \mathcal{M}_{ij}^{n,m-1} \tilde{\delta} p_{\beta M,ij'}^{n,m} \Big] = 0, \\ D_{p_{\beta F,i}} \mathcal{M}_{ij}^{n,m-1} + \sum_{j'} \Big[D_{p_{\alpha M,ij'}} \mathcal{M}_{ij}^{n,m-1} \hat{\delta} p_{\alpha M,ij'}^{n,m} + D_{p_{\beta M,ij'}} \mathcal{M}_{ij}^{n,m-1} \hat{\delta} p_{\beta M,ij'}^{n,m} \Big] = 0, \\ \mathcal{M}_{ij}^{n,m-1} + \sum_{j'} \Big[D_{p_{\alpha M,ij'}} \mathcal{M}_{ij}^{n,m-1} \bar{\delta} p_{\alpha M,ij'}^{n,m} + D_{p_{\beta M,ij'}} \mathcal{M}_{ij}^{n,m-1} \bar{\delta} p_{\beta M,ij'}^{n,m} \Big] = 0. \end{cases} \tag{2.21}$$

The result is that

$$\delta p_{\xi M,ij}^{n,m} = \tilde{\delta} p_{\xi M,ij}^{n,m} \delta p_{\alpha F,i}^{n,m} + \hat{\delta} p_{\xi M,ij}^{n,m} \delta p_{\beta F,i}^{n,m} + \bar{\delta} p_{\xi M,ij}^{n,m}. \tag{2.22}$$

We thus modify step 2(a) of the Newton algorithm by first solving (2.21). The fracture δ-pressures are then given by solving the fracture equations of (2.20), using implicitly the definition (2.22). Finally, we explicitly use the fracture δ-pressures and (2.22) to update the matrix δ-pressures.

3 Some computational results

In this section we present some computational results that illustrate the dual-porosity model and its ability to approximate the mesoscopic model. (See also [4].)

3.1 Single-phase

We consider a simulation representing, for example, primary depletion of oil from a petroleum reservoir. In order to be able to solve the mesoscopic model, we restrict to two spatial dimensions and a relatively small system. However, we consider more generally the model of Section 1.1 with gravitational effects, as described in detail in [3].

The flow is not given by a potential field; however, we can define the pseudo-potential

$$\Phi = \int_{p_0}^{p} \frac{dP}{\rho(P)\,g} - z(x) = \frac{1}{\rho_0 gc}[1 - e^{-c(p-p_0)}] - z(x) = \frac{1}{\rho_0 gc}\left(1 - \frac{\rho_0}{\rho}\right) - z(x), \tag{3.23}$$

using (1.3), so that

$$\rho = \frac{\rho_0}{1 - \rho_0 gc(\Phi + z(x))}. \tag{3.24}$$

Then

$$\rho(p)\,g\,\nabla\Phi = \nabla p - \rho(p)\,g\,\nabla z(x)$$

is a nonlinear relation giving the Darcy velocity after multiplication by k/μ. After multiplication by $\rho(p)$, we have the mass flux as $\dfrac{\rho(p)^2 gk}{\mu}\nabla\Phi$, which replaces the $\dfrac{k}{\mu c}\nabla\rho$ terms in (1.4)–(1.8). The fracture and matrix pseudo-potentials are defined by

$$\Phi_F(t,x) = \frac{1}{\rho_0 gc}\left(1 - \frac{\rho_0}{\rho_F(t,x)}\right) - z(x), \tag{3.25}$$

$$\Phi_M(t,x,y) = \frac{1}{\rho_0 gc}\left(1 - \frac{\rho_0}{\rho_M(t,x,y)}\right) - z(x + y - y_c), \tag{3.26}$$

and the boundary condition in (1.8) is replaced by

$$\Phi_M(t,x,y) = \Phi_F(t,x) \quad \text{on } (0,T)\times\Omega\times\partial M, \tag{3.27}$$

giving continuity of pseudo-potential, where the reference value is defined for $x \in \Omega$ by

$$\int_M \frac{\rho_0}{1 - \rho_0 gc\,(\Phi_F - \Phi_0 + z(x + y - y_c))}\,dy = \int_M \frac{\rho_0}{1 - \rho_0 gc\,(\Phi_F + z(x))}\,dy = |M|\rho_F. \tag{3.28}$$

We assume the fluid is an oil with $\rho_0 = 0.8\,\mathrm{g/cm^3}$, $p_0 = 0\,\mathrm{psi}$, $c = 10^{-5}\,\mathrm{psi^{-1}}$, and $\mu = 2\,\mathrm{cp}$. Let the entire reservoir be 8 meters long and 8 meters deep. Let there be 16 matrix blocks filling the reservoir, each 2 meters by 2 meters, with $\phi_M = 0.2$ and $k_M = 1\,\mathrm{millidarcy}$. The fractures are 100 micrometers wide, with $\phi_F = 1$ and $k_F = 844\,\mathrm{darcy}$. We have used the usual formula for the permeability of the fracture as the width squared divided by 12; this formula comes from considering Stokes flow between parallel plates. For the dual-porosity model, the macroscopic fracture porosity ϕ^* is given by the geometry, and the permeability $k^* = 42.2\,\mathrm{millidarcy}$ is approximately just k_F times the fracture width divided by the matrix block length in two dimensions (see [4]).

A well is placed in the upper left corner of the reservoir. The initial pressure there is 4000 psi, and the fluid is in gravitational equilibrium. The well pressure is dropped linearly to 3000 psi in 10 days.

We show the results from four simulations, one on the mesoscopic scale and three on the dual-porosity, macroscopic scale. We used a Galerkin finite element spatial discretization with piecewise

continuous, bilinear basis functions. There were 89×89 (7921) grid points for the mesoscopic solution. We used 3×3, 4×4, and then 8×8 grid points for the fracture calculation of the dual porosity simulation, and 21 points for the calculation in each matrix block, yielding a total of 189, 336, and 1344 grid points, respectively. The linearization techniques introduced earlier in this paper were used to solve the dual-porosity systems. It is difficult to compare the performance of different numerical techniques, since it depends on the specific way the code is implemented; however, it should be noted that the mesoscopic solution required about a half hour to solve accurately because it is so very ill-conditioned, but the much better conditioned dual-porosity simulations took only a few seconds.

In Figure 2, we show the oil production rates as a function of time. All four simulations predicted roughly the same production history, both in the draw-down phase and in the re-equilibration stage after 10 days.

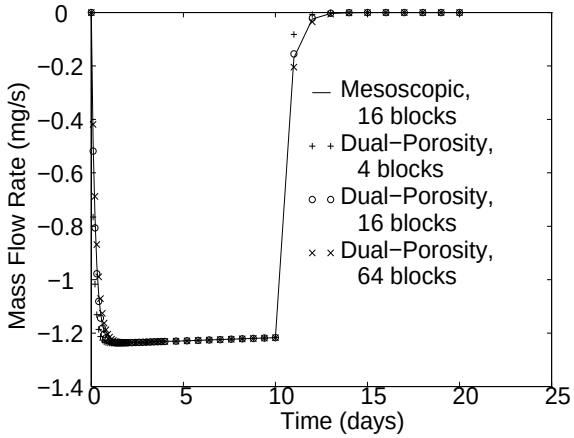

Figure 2: Oil production rates as a function of time.

In Figure 3, we show the mesoscopic oil density contours (actually, the densities minus 0.824 and multiplied by 10,000). As can be seen, pressure is reduced most strongly in the fractures between the matrix blocks, and also most strongly near the well in the upper left. Oil in the interior of the matrix blocks takes longer to be produced than oil in the fractures and near the surface of the blocks. Note also the strong influence of gravity in these simulations.

In Figure 4, we show the dual-porosity matrix oil density contours when there are 16 fracture grid points (so there are also the correct number of matrix blocks, 16). As can be seen, except near the well, the dual-porosity model has captured the flow of the system quite accurately. Since the well itself is a spatially local feature of the reservoir, it should not be expected to be approximated as well by the dual-porosity model; however, there is *not* a pollution of the solution away from the well.

In Figures 5–6, we show the dual-porosity matrix oil density contours when there are 9 and 64 fracture grid points. Now the number of matrix blocks in the dual-porosity model is at variance with the true number. Nevertheless, the average behavior of the system has been captured quite well.

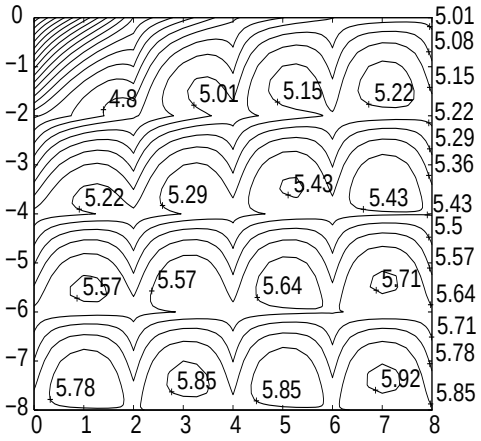

Figure 3: Mesoscopic density contours [in $(\times 10^{-4} + .824)\mathrm{g/cm}^3$] as a function of position (in m).

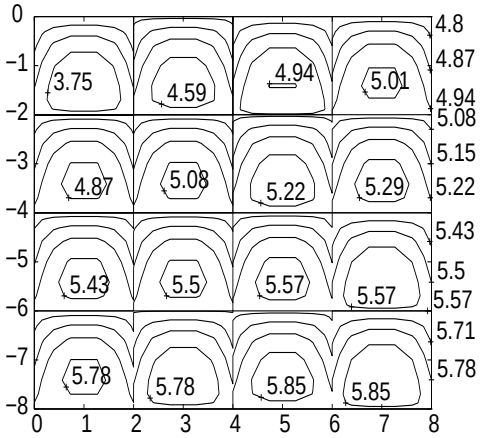

Figure 4: Dual-porosity matrix density contours [in $(\times 10^{-4} + .824)\mathrm{g/cm}^3$] for the 4×4 fracture discretization.

3.2 Two-phase

We now consider simulating a petroleum water-flood. Water is injected into the reservoir at some rate through an injection well. The water displaces oil, and oil and some of the water is recovered at a second, production well. We restrict attention to a single matrix block in two spatial dimensions so that the mesoscopic equations can be solved accurately. We consider three cases wherein the fracture width is either 200 or 100 micrometers and the wells are placed either horizontally or vertically.

Assume that the wetting phase α is water with $\rho_\alpha = 1.0\,\mathrm{g/cm}^3$ and $\mu_\alpha = 0.5\,\mathrm{cp}$, and the β

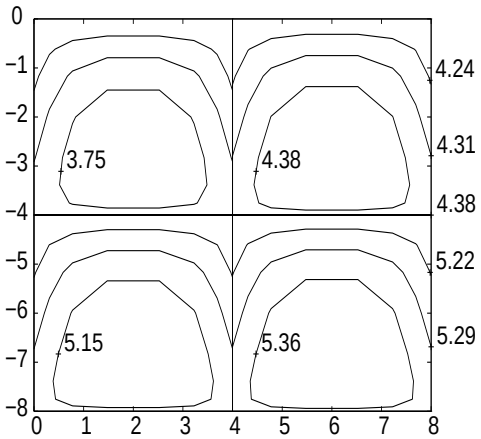

Figure 5: Dual-porosity matrix density contours [in $(\times 10^{-4} + .824)\mathrm{g/cm}^3$] for the 3×3 fracture discretization.

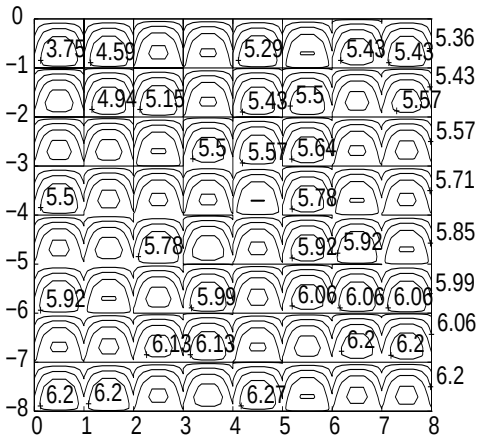

Figure 6: Dual-porosity matrix density contours [in $(\times 10^{-4} + .824)\mathrm{g/cm}^3$] for the 8×8 fracture discretization.

phase is an oil with $\rho_\beta = 0.8\,\mathrm{g/cm^3}$ and $\mu_\beta = 2.0\,\mathrm{cp}$. The reservoir and its single block is a square of size ℓ by ℓ where $\ell = 2\,\mathrm{meters}$. The fracture width δ is assumed to be either 200 micrometers or 100 micrometers (but note that by our conventions, only half of the fractures actually reside in the reservoir). Assume that $\phi_M = 0.2$, $k_M = 4\,\mathrm{millidarcy}$, $\phi_F = 1.0$, ϕ^* is given by the geometry as either 0.0002 or 0.0001 , $k_F = \delta^2/12$ is either $3,377,000$ or $844,000\,\mathrm{millidarcy}$, and $k^* = \delta^3/12\ell$ is either 337 or $42\,\mathrm{millidarcy}$. We take the residual saturations in the fractures as $S_{r\alpha F} = 0$ and $S_{r\beta F} = 0$, and in the matrix as $S_{r\alpha M} = 0.25$ and $S_{r\beta M} = 0.3$; thus, $0.25 \le S_{\alpha,M} \le 0.7$. The relative permeability and capillary pressure functions take the form

$$k_{r\alpha F}(s) = s, \qquad k_{r\beta F}(s) = 1 - s, \qquad \text{and} \quad p_{cF}(s) = 4(1-s)^{200}\,\mathrm{psi},$$
$$k_{r\alpha M}(s) = \left(\frac{s - 0.25}{0.75}\right)^2, \quad k_{r\beta M}(s) = \left(\frac{0.7 - s}{0.7}\right)^2, \quad \text{and} \quad p_{cM}(s) = 4\left(\frac{0.7 - s}{0.45}\right)^4\,\mathrm{psi}.$$

The capillary pressure functions are plotted in Figure 7.

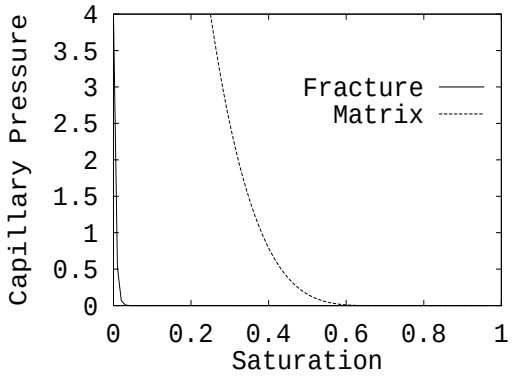

Figure 7: The capillary pressure functions in psi.

The wells are configured to lie on opposite edges of the reservoir, either horizontally or vertically. Water is injected at a rate of 20 pore-volumes per year from below if the wells are horizontal, and from the left if they are vertical.

As we will see in our simulations, there are several physical phenomena that influence the movement of the fluids. Oil is recovered from the matrix primarily through capillary imbibition of water. This displaces oil, which can then be recovered at the production well. As water is imbibed into the matrix, however, it lowers the relative permeability to oil; consequently, an insulating boundary layer is produced that inhibits further oil displacement. It is the trade-off between these two effects that primarily determines the behavior of the reservoir. Another significant phenomenon is the gravitational force acting on the fluids; oil tends to "float" above water. This helps to break down the insulating boundary layer. Finally, a less important, but as we will see, a sometimes significant phenomenon is the presence of a pressure gradient across the block. This gives rise to "viscous" forces that tend to move the fluids to one side of the matrix block, again breaking down the insulating boundary layer. This last effect is absent in the dual-porosity model, and we will need to introduce a "viscous" dual-porosity model as a simple modification; see also [1], [2], and [8].

The oil recovery curves shown in Figure 8 apply to Case 1, in which the fracture is relatively wide (200 micrometers) and the well is symmetric with respect to gravity (i.e., horizontal). Virtually no potential gradient can be supported in the fractures because they are so wide. Since the dual-porosity model assumes that the potentials do not vary in space over the boundary of the matrix block, we see very good agreement in this case between the mesoscopic and dual-porosity models in the amount of fluid produced from the reservoir. The viscous dual-porosity model is also in good agreement.

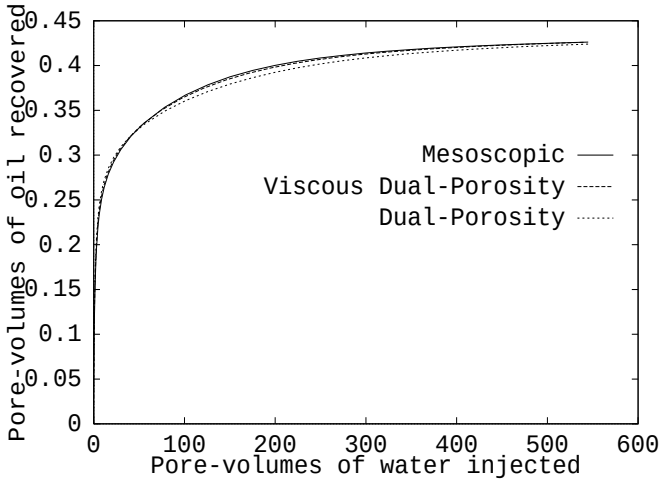

Figure 8: Oil produced as a function of water injected (200 micrometer fracture, horizontal wells).

In Case 2 we restrict the fracture width to 100 micrometers (and keep horizontal wells). As shown in Figure 9, the mesoscopic and dual-porosity models exhibit good agreement in oil recovery only for early time; at later times they predict significantly different recovery rates.

In Figure 10 we show the water saturation contours in the matrix for the simulation at 10 days. (The dual-porosity results are the average of all matrix blocks simulated across the reservoir.) The agreement looks quite good, but a careful inspection will reveal that water has been pushed upwards from the injection well to the production well in the mesoscopic model. This is due to the slight but significant pressure gradient across the block. Our viscous dual-porosity model accounts properly for this effect, and we now define it.

The viscous dual-porosity model is given by replacing the boundary condition on the matrix block in (2.17) by

$$\Phi_{\xi M}(t,x,y) = \Phi_{\xi F}(t,x) + \nabla_x \Phi_{\xi F}(t,x)\cdot(y-y_c), \quad \text{on } (0,T)\times\Omega\times\partial M, \tag{3.29}$$

Although the gradient creates a coupling of more than one fracture grid point to each matrix block, the number is small, and the techniques introduced above can be used to decouple the matrix computations from the fracture computation. It is believed that the source term in the fracture equations should be modified as well; however, this was not done in the simulations here.

Finally, in Case 3 we consider a more challenging problem that exhibits all of the main phenomenon influencing fluid movement. We take again a 100 micrometer fracture, but drive the

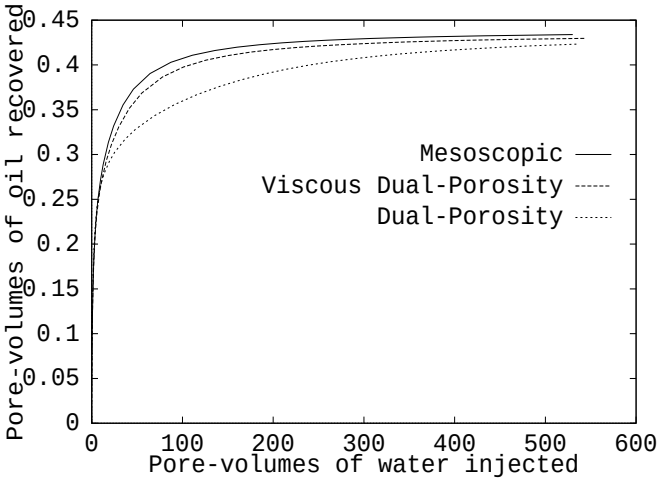

Figure 9: Oil produced as a function of water injected (100 micrometer fracture, horizontal wells).

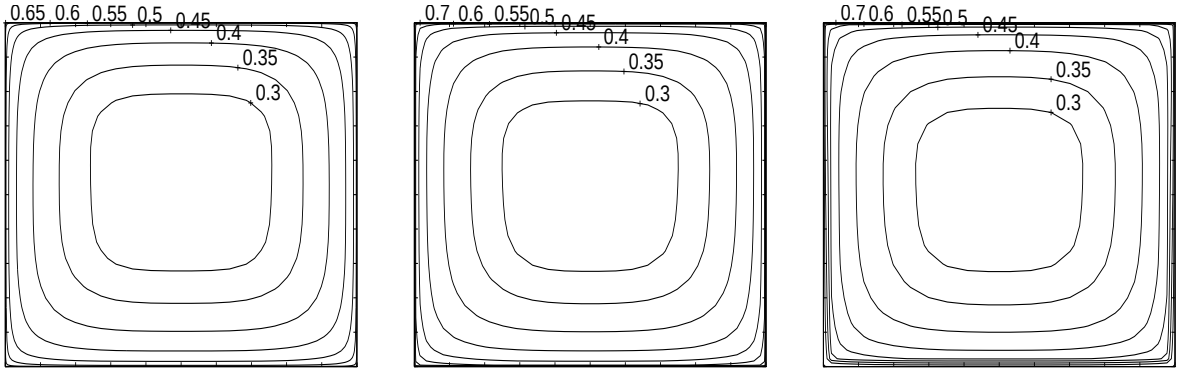

Figure 10: Water saturation at 10 days (100 micrometer fracture, horizontal wells).

system with vertical wells. The wells are now asymmetric with respect to gravity. The recovery curves in Figure 11 show that the dual-porosity model is only able to predict oil production accurately only for early time when imbibition dominates. For later times, the viscous model is needed to obtain accurate recovery curves.

In Figures 12–16, we show the history of the simulation for the three models. Starting from gravitational equilibrium, we see seepage left to right into the fracture at 0.1 day, with water sliding preferentially under oil because of gravity. The dual-porosity model cannot see these effects, but the viscous model does an admirable job. The insulating layer of water around the boundary of the matrix block can be seen in all three models by 1 day. By 10 and 100 days, we start to see the gravitational and viscous effects showing up in the mesoscopic model; these are well approximated in the viscous model. The dual-porosity model must maintain a symmetric solution, and so it approximates well only gravity. By 1000 days, there is very little oil left in the matrix block. The mesoscopic model exhibits water coning, where water creeps up from below into the production

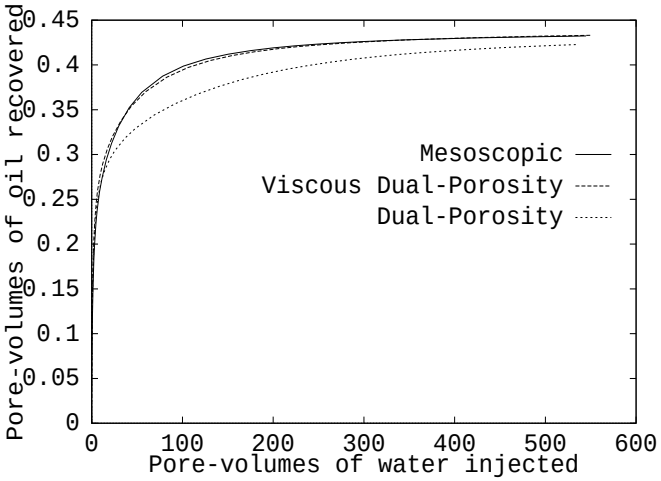

Figure 11: Oil produced as a function of water injected (100 micrometer fracture, vertical wells).

well. The viscous model cannot predict this effect, but is reasonable otherwise. The dual-porosity model itself cannot see the pronounced break-down in the insulating boundary layer to the right of the block.

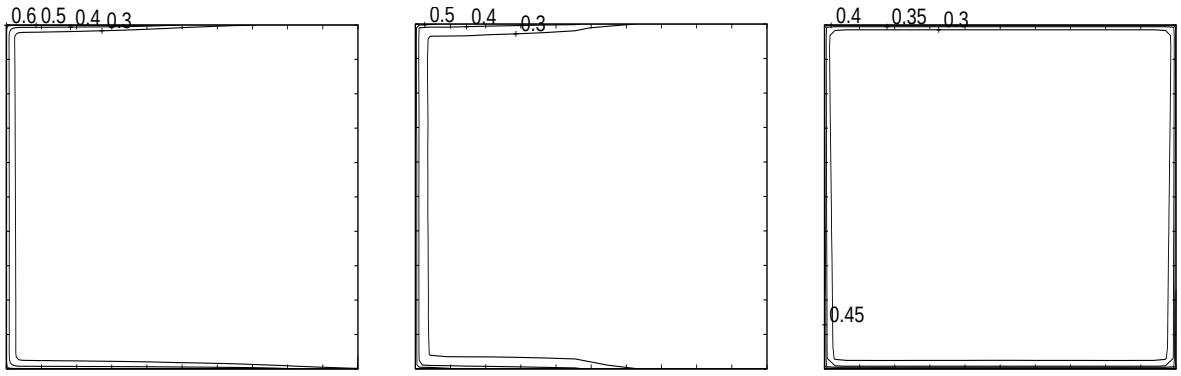

Mesoscopic Viscous dual-porosity Dual-porosity

Figure 12: Water saturation at 0.1 day (100 micrometer fracture, vertical wells).

It is an open question how to derive to the viscous dual-porosity model from homogenization. However, homogenization has given us the basic model from which we can make a simple modification to improve the simulation of two-phase flow, so that late time predictions can be made accurately.

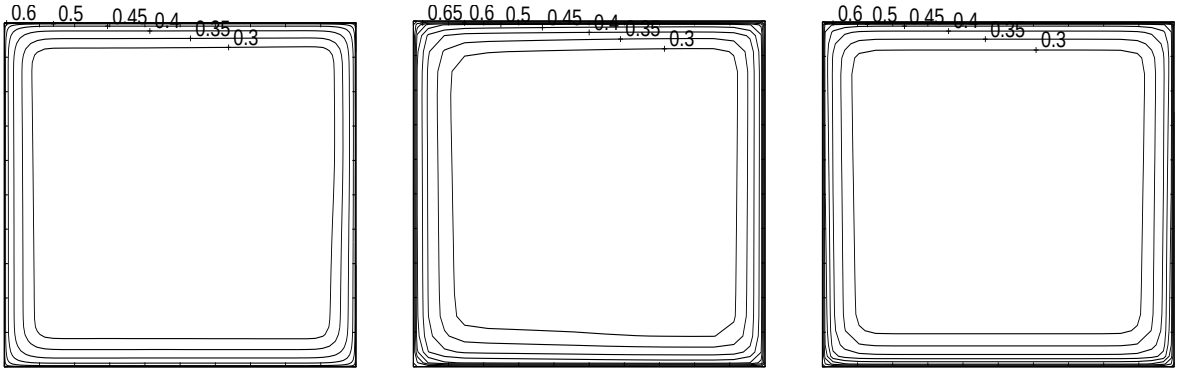

Mesoscopic Viscous dual-porosity Dual-porosity

Figure 13: Water saturation at 1 day (100 micrometer fracture, vertical wells).

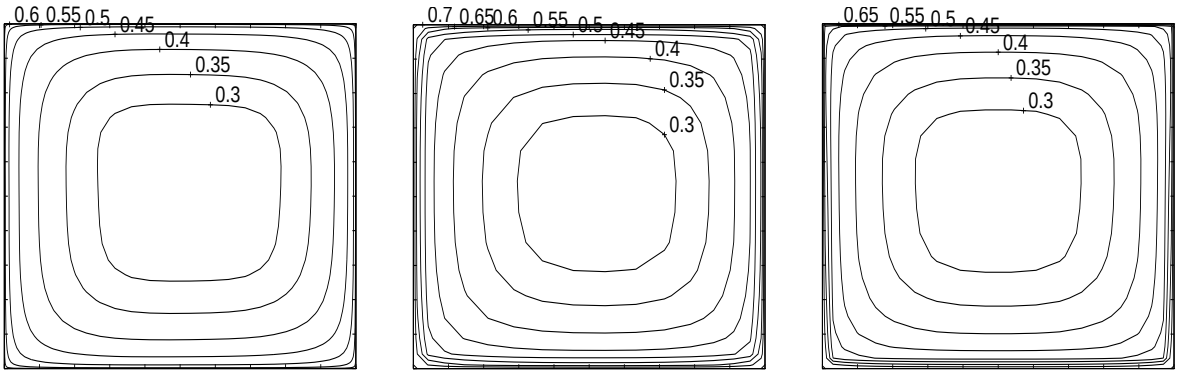

Mesoscopic Viscous dual-porosity Dual-porosity

Figure 14: Water saturation at 10 days (100 micrometer fracture, vertical wells).

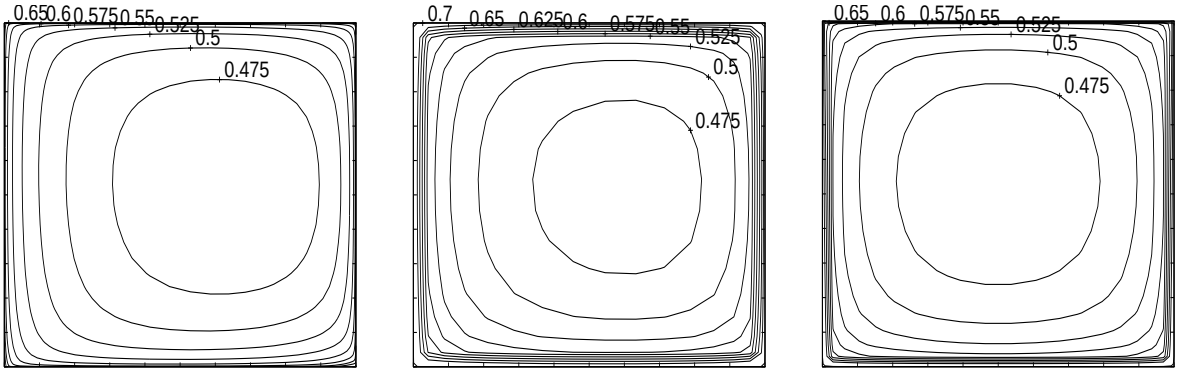

Mesoscopic Viscous dual-porosity Dual-porosity

Figure 15: Water saturation at 100 days (100 micrometer fracture, vertical wells).

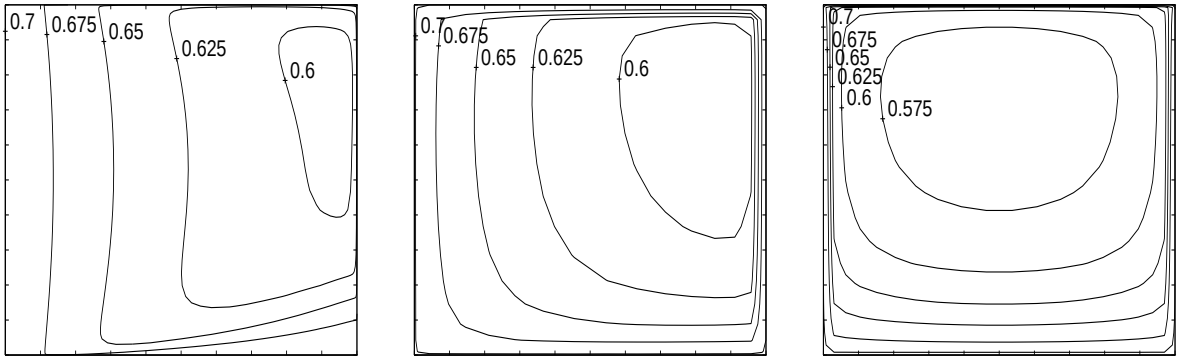

Mesoscopic Viscous dual-porosity Dual-porosity

Figure 16: Water saturation at 1000 days (100 micrometer fracture, vertical wells).

References

[1] T. Arbogast. Analysis of the simulation of single phase flow through a naturally fractured reservoir. *SIAM J. Numer. Anal.*, 26:12–29, 1989.

[2] T. Arbogast. On the simulation of incompressible, miscible displacement in a naturally fractured petroleum reservoir. *R.A.I.R.O. Modél. Math. Anal. Numér*, 23:5–51, 1989.

[3] T. Arbogast. Gravitational forces in dual-porosity systems. I. model derivation by homogenization. *Transport in Porous Media*, 13:179–203, 1993.

[4] T. Arbogast. Gravitational forces in dual-porosity systems. II. computational validation of the homogenized model. *Transport in Porous Media*, 13:205–220, 1993.

[5] T. Arbogast, J. Douglas, and U. Hornung. Modeling of naturally fractured reservoirs by formal homogenization techniques. In R. Dautray, editor, *"Frontiers in Pure and Applied Mathematics"*, pages 1–19, Amsterdam, 1991. Elsevier.

[6] T. Arbogast, J. Douglas, Jr., and U. Hornung. Derivation of the double porosity model of single phase flow via homogenization theory. *SIAM J. Math. Anal.*, 21:823–836, 1990.

[7] G. I. Barenblatt, I. P. Zheltov, and I. N. Kochina. Basic concepts in the theory of seepage of homogeneous liquids in fissured rocks (strata). *J. Appl. Math. Mech.*, 24:1286–1303, 1960.

[8] J. D. Cook and B. D. Showalter. Microstructure diffusion models with secondary flux. *Jour. Math. Anal. Appl*, 189:731–756, 1995.

[9] J. Douglas and T. Arbogast. Dual-porosity models for flow in naturally fractured reservoirs. In J. Cushman, editor, *Dynamics of Fluids in Hierarchical Porous Media*, pages Chapter VII, 177–221. Academic Press, 1990.

[10] J. Douglas, Jr., J. L. Hensley, and T. Arbogast. A dual-porosity model for waterflooding in naturally fractured reservoirs. *Comp. Meth. in Appl. Mech. and Engng.*, 873:157–174, 1991.

[11] J. Warren and P. Root. The behavior of naturally fractured reservoirs. *Soc. Petroleum Engr. J.*, 3:245–255, 1963.